A Generic Power Converter Sizing Framework for Series-Connected DC Offshore Wind Farms

Marten Pape, *Graduate Student Member, IEEE*, and Mehrdad Kazerani, *Senior Member, IEEE*

***Abstract*—Wind farms featuring a series-connected dc collection system have been shown to offer advantages in terms of total conversion efficiency and amount of offshore-deployed equipment. To ensure proper exploitation of these benefits, it is necessary to determine the ratings of wind turbine converters. These ratings must be sufficient to cover the expected operating conditions over the life of the wind farm, without unnecessarily oversizing the equipment. As shown in this article, the variable string current results in an interdependence of operating points among wind turbines that has to be considered for sizing these converters. This article proposes a generic sizing framework for such single-string, series-connected dc wind farms. This framework is applied to three wind farm configurations featuring differential power processing, voltage-source converters, and diode-bridge rectifiers and buck converters. Finally, a case study for a 450 MW offshore wind farm demonstrates the implementation of this sizing methodology and quantifies the design tradeoffs between converter ratings and energy production enabled from those converters. In two of the studied wind farm configurations, significant rating reductions are achievable while still avoiding energy curtailment for $>$99.7% of the energy production of an equivalent ac wind farm.**

***Index Terms*—Converter ratings, converter sizing, dc collection systems, dc–dc power conversion, offshore wind farms, series-connected collection system, wind energy.**

I. Introduction

With increasing deployment of offshore wind farms, there is a heightened interest in minimizing the cost of their energy generation. Cost reduction can be achieved from the optimization of overall conversion efficiency and reduction of electric equipment required for offshore collection and transmission systems [1]. Conventional offshore wind farms are based on an internal medium-voltage ac grid. For wind farms with longer distances to shore, HVdc transmission systems are used to facilitate efficient energy transmission to shore [2]. In [1], the replacement of the offshore ac collection system with various configurations of dc collection systems was analyzed and found increasingly superior to ac collection systems as distance to shore increases. The dc collection systems can be realized using a parallel, series, or parallel connection of series-connected wind turbines [3]. Furthermore, the choice of wind turbine power converter topology significantly influences the overall wind turbine design. For wind farms with a series-connected dc collection system, as shown in Fig. 1, conversion systems based on a high-frequency isolation transformer and ac–ac converter [4], [5], reduced matrix converter [6], thyristor converter [7], current-source converter [8]–[11], diode-bridge rectifiers and boost converter [12], diode-bridge rectifier and buck converter [13], diode-bridge rectifier and partial power processing converters [14], diode-bridge rectifiers and excitation control of wound-rotor synchronous generators [15], [16], diode-bridge rectifiers and power factor correction [17], diode-bridge rectifiers and input-series output-series single-active bridge converters [18], modular multilevel converters [19], [20], voltage-balancing circuits [21], voltage-source converters (VSCs) [11], [22], VSCs and full-bridge converter [23], VSCs and single-active bridge converters [24], [25], VSCs and double full bridge double tapped inductor converter [26], and VSCs, dual-active bridge converters and energy storage [27], have been studied.

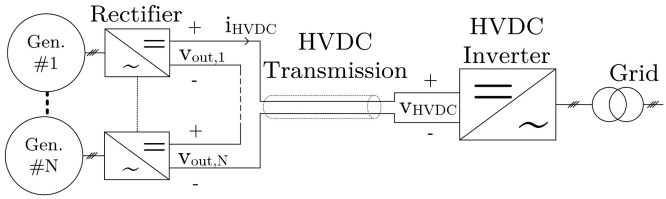

Fig. 1. General structure of a single-string, series-connected dc wind farm. ("Gen." = Generator).

Typically, the HVdc voltage and current are both a function of the operating states of all wind turbines in single-string, series-connected wind farms [13], [22], unlike with conventional wind farms where the HVdc voltage is fixed [28]. As a result, the operating conditions of each wind turbine converter are influenced by its operating points, as well as those of all other wind turbines in the farm. Consequently, the choice of component ratings for a wind turbine converter is dependent on the expected operating points of its wind turbine and simultaneous operating points of all other wind turbines in the farm. Several works have explored the valid operating regions for particular wind farm configurations based on sample sets of wind turbine operation [11], [22], [29]. For conventional wind turbines with ac voltage output, collection system buses operate at fixed voltage and the operating points of one wind turbine converter do not affect

Manuscript received February 1, 2021; revised May 13, 2021 and July 9, 2021; accepted August 10, 2021. Date of publication August 20, 2021; date of current version October 15, 2021. This work was supported by the Natural Sciences and Engineering Research Council of Canada. Recommended for publication by Associate Editor A. K. Gupta. *(Corresponding author: Marten Pape.)*

The authors are with the Department of Electrical and Computer Engineering, University of Waterloo, Waterloo, ON N2L 3G1, Canada (e-mail: marten.pape@uwaterloo.ca; mkazerani@uwaterloo.ca).

Color versions of one or more figures in this article are available at https://doi.org/10.1109/TPEL.2021.3106578.

Digital Object Identifier 10.1109/TPEL.2021.3106578

those of other wind turbine converters. Hence, converter ratings are chosen based on the operating conditions at full-power operation. Most previous studies on series-connected dc wind farms have been based on a predetermined set of converter ratings. Zhang *et al.* [30], [31], Guo *et al.* [32], Shi *et al.* [33], and Lakshmanan *et al.* [34] discussed various control approaches utilizing the modification of wind farm operating points and/or wind power curtailment to limit extreme operating points and overvoltage conditions in series-connected wind farms based on fixed component ratings. In [11], aerodynamic wake modeling is applied to a series-parallel wind farm based on VSCs to demonstrate the adequacy of chosen component ratings and maximize energy production. A similar wake model is used in [34]. In [27] and [35], the application of energy storage in wind turbines is considered to limit undervoltage and overvoltage conditions. Bahirat and Mork [27] recognized the probabilistic nature of energy storage capacity requirements, yet associated likelihoods are not derived systematically.

In contrast with the previous works that are largely focused on optimizing wind farm operation based on a fixed and chosen set of wind farm component ratings, or rely on assumed likelihoods for extreme operating conditions, component ratings are considered variable in this article. A methodology to aid determining desirable component ratings is proposed. In particular, this article contributes a methodology for sizing the voltage and current ratings of wind turbine converters' components in single-string, series-connected wind farms. This methodology allows capturing the influence of wind turbine converter topology, wind conditions at the chosen site, and wind farm layout on wind turbine converter ratings. The methodology determines the amount of annual energy curtailment due to converter rating limitations in order to allow for optimizing the tradeoff between converter ratings and related annual energy curtailment.

The rest of this article is organized as follows. In Section II, challenges in determining voltage and current ratings in converters for series-connected dc wind farms are discussed. Based on that, Section III introduces a generic sizing framework applicable to converter topologies in single-string, series-connected wind farms that considers full and partial operational range sizing. This generic framework is then applied to wind turbine converter configuration featuring differential power processing capabilities [14], voltage-source converters, and diode-bridge rectifiers and buck converters in Sections IV, V, and VI, respectively. The theoretical relations found in that section are then used in a case study in Section VII. This case study examines a total of 17 candidate converter rating sets across the three wind farm configurations for a fictional 450 MW wind farm located off the German coast in the North Sea and predicts the annual energy curtailment due to finite converter rating. Finally, Section VIII concludes this article.

II. Converter Sizing Challenges in Series-Connected DC Wind Farms

In conventional wind turbines featuring a full-scale back-to-back VSC for fixed ac voltage output (as shown in Fig. 2) the determination of component voltage and current ratings (sizing) tends to be governed by the system operation at full power. For example, IGBT voltage ratings of a two-level VSC are based on the nominal voltage of the internal dc bus, as well as a certain safety margin. IGBT current ratings are largely based on the expected currents at full-power operation. Overall, the sizing of wind turbine converters is independent of expected or actual operating states of neighboring wind turbines.

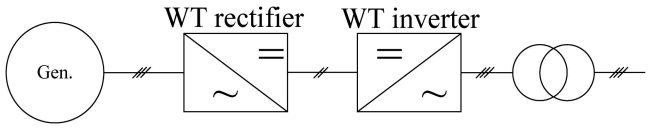

Fig. 2. Conventional wind turbine electric power conversion system.

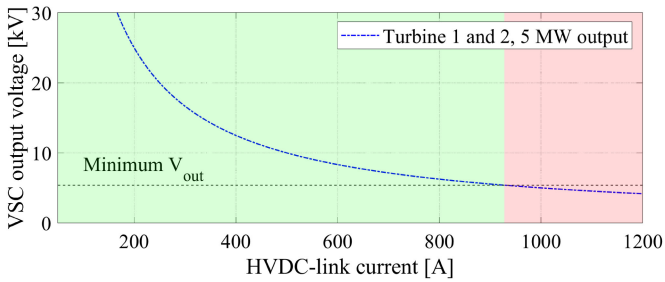

Fig. 3. Illustration of required dc output voltages and valid HVdc-link currents of a wind farm with two wind turbines featuring VSCs as rectifiers operating at rated output powers. Green area: valid rectifier operating points; pink area: minimum VSC output voltage criterions violated.

In contrast, the sizing of wind turbine converters for series-connected dc wind farms is dependent on operating states of neighboring wind turbines, and not necessarily entirely based on full-power operating conditions. Fig. 1 shows the general structure of a single-string, series-connected dc Wind Farm, consisting of N wind turbines and incorporating an HVdc link. To illustrate the difference, this section discusses two sample operating conditions of a single-string series-connected wind farm using a VSC as rectifier in each wind turbine. This wind farm features two 5 MW wind turbines and 3.3 kV generators. Furthermore, it is considered that the minimum VSC dc output voltage $V_{\mathrm{out},n}$, is equal to $2\sqrt{2}/\sqrt{3}$ times the generator line-to-line terminal voltage to ensure PWM operation in the linear region is maintained and overmodulation is avoided [36], ignoring effects of the stator impedance, as well as reactive power flows.

In the first operating condition, both wind turbines operate at rated power. To satisfy the minimum VSC dc output voltage requirement, both VSCs have to operate with an output voltage of at least 5.4 kV, as shown in Fig. 3. This results from both generators operating at rated speed and ac voltage. In Fig. 3, the green area indicates the range of HVdc-link current that can be chosen, such that the VSC output voltage is higher than 5.4 kV at the given operating condition. The pink area indicates a range of HVdc-link currents that would require a VSC output voltage below its minimum output voltage, in order to operate with rated output power. As a result, the string current I_{HVdc} must (be controlled to) be equal to or less than 928 A. Hence,

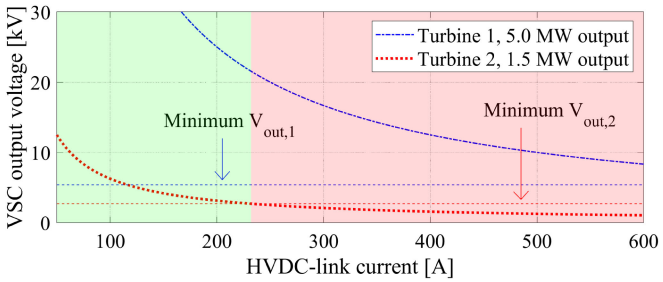

Fig. 4. Illustration of required dc output voltages and valid HVdc-link currents of a wind farm with two wind turbines featuring VSCs as rectifiers operating at differing output powers. Green area: valid rectifier operating points; pink area: minimum VSC output voltage of rectifier 2 violated.

the VSCs' IGBTs must be rated to withstand a voltage of at least 5.4 kV plus a safety margin.

Now considering a second operating condition at lower total power output, it will be shown that a higher IGBT voltage rating is required. Here, wind turbine 1 operates at rated power (5 MW), while wind turbine 2 operates at 30% rated power (1.5 MW). As shown in Fig. 4, the minimum VSC output voltage for wind turbine 2 drops, as the generator speed and ac voltage is lower at wind conditions resulting in 1.5 MW output power for a variable-speed wind turbine operating at optimal tip-speed ratio. The maximum string current I_{HVdc} corresponds to the point where a VSCs output voltage reaches its minimum value first as string current is increased. In this case, the lower minimum output voltage of wind turbine 2 requires the string current I_{HVdc} to be at most 232 A to satisfy the minimum dc output voltage requirement of the VSC of wind turbine 2, as seen in Fig. 4. This significantly lowers the string current and forces the VSC of wind turbine 1 to operate at a significantly elevated output voltage level of at least 21.5 kV. Accordingly, the VSCs' IGBTs would have to be rated to at least 21.5 kV to allow this operating condition to exist without power curtailment. In typical wind farm designs, each wind turbine would be installed with the same converter ratings, including the higher voltage rating for its VSCs.

This example demonstrates that in series-connected dc wind turbines, the sizing of wind turbine converters introduces an interdependency among wind turbines and is not entirely based on operation at full power.

III. Generic Converter Sizing Framework

In this section, a generic wind turbine converter sizing framework for single-string, series-connected dc wind farms is developed that addresses the interdependencies outlined in Section II.

A. System Description

This section considers the general structure of a single-string, series-connected dc Wind Farm shown in Fig. 1. The output power of wind turbine n, P_n, is generated according to internal control laws at a particular generator line-to-line voltage $V_{\mathrm{gen},n}$ and electrical frequency $f_{\mathrm{gen},n}$. A rectifier is used in each wind turbine to convert the ac to dc output power, such that the output voltage of wind turbine n, $V_{\mathrm{out},n}$, adheres to

$$V_{\mathrm{out},n} = \frac{P_n}{I_{\mathrm{HVdc}}} \tag{1}$$

where I_{HVdc} is the HVdc-link current. In the rest of this article, the states of wind turbine n in a string of N turbines are represented in vector $\boldsymbol{S_n}$

$$\boldsymbol{S_n} = \left[\, \boldsymbol{S_{T,n}}\ \boldsymbol{S_{I,n}} \,\right]^T. \tag{2}$$

This vector consists of the converter terminal state vector $\boldsymbol{S_{T,n}}$ and converter internal state vector $\boldsymbol{S_{I,n}}$. While $\boldsymbol{S_{I,n}}$ is specific to the chosen converter topology, $\boldsymbol{S_{T,n}}$ is generally defined as

$$\boldsymbol{S_{T,n}} = \left[\, P_n\ V_{\mathrm{gen},n}\ f_{\mathrm{gen},n}\ I_{\mathrm{HVdc}} \,\right]^T. \tag{3}$$

For each wind turbine rectifier type, a steady state, topology-specific relationship between converter terminal and internal states, and rectifier output voltage $V_{\mathrm{out},n}$ can be established

$$V_{\mathrm{out},n} = f\left(\boldsymbol{S_n}\right). \tag{4}$$

For a particular converter topology, (4) would model the complete steady-state internal relationships of such converter, unlike in (1) which expresses $V_{\mathrm{out},n}$ based on converter terminal quantities. Equation (4) will be used to consider converter component limitations for the purpose of sizing the converter. In this article, it is being assumed that the converters in all wind turbines of a farm have the same component ratings.

In a single-string series-connected dc wind farm, I_{HVdc} is actively controlled by the HVdc inverter station [13]. As a result, the HVdc-link voltage V_{HVdc} becomes

$$V_{\mathrm{HVdc}} = \frac{1}{I_{\mathrm{HVdc}}} \sum_{n=1}^{N} P_n. \tag{5}$$

The HVdc-link current reference is derived from an HVdc-link current scheduling law specific to the topology and design of wind farm and power converter. Various objectives can be implemented with such law, such as eliminating an offshore-onshore communication link [13], maintaining a constant HVdc-link voltage [13], minimizing processed power [14], maximizing energy yield (compare to [11]), or minimizing required converter ratings. Once an HVdc-link current scheduling law has been selected, all basic electrical system states are known as per (1)–(3) and (5), other than P_n, $V_{\mathrm{gen},n}$, and $f_{\mathrm{gen},n}$ that depend on the incoming wind conditions. Unlike with conventional offshore wind farms featuring an ac voltage collection system, wind turbine and HVdc link voltages, $V_{\mathrm{out},n}$ and V_{HVdc} are not held constant. Instead, they all are functions of wind turbine output power P_n and the HVdc-link current I_{HVdc}.

B. Generic Sizing Problem Formulation

The choice of wind turbine rectifier topology, converter ratings, and HVdc-link voltage rating introduce constraints on the range of feasible HVdc-link currents. This directly affects wind turbine output voltages, particularly in the presence of wind speed and output power differences within the series string, as illustrated in Section II.

The rectifying converter can introduce minimum and/or maximum constraints on wind turbine output power $P_n(\boldsymbol{S_n})$ or wind turbine output voltage $V_{\mathrm{out},n}(\boldsymbol{S_n})$. Some of these constraints can depend on the wind turbine's current state $\boldsymbol{S_n}$. The limitations result from the component ratings within the converter, and from the choice of converter topology.

In addition, the HVdc-link insulation rating introduces a maximum possible HVdc-link voltage constraint $\overline{V_{\mathrm{HVdc},R}}$ and I_{HVdc} should not exceed values that cause an excessive HVdc-link voltage. Similarly, there is a maximum rated HVdc-link current $\overline{I_{\mathrm{HVdc},R}}$. Furthermore, wind turbine startup and shutdown can introduce additional constraints on converter sizing or HVdc link operation [37], as well as wind farm configuration-specific fault handling schemes and certain fault-ride through schemes. For example, certain wind turbine output converter voltage or current ratings can be required to facilitate wind turbine startup [37], or withstand faults in the dc collection system [38].

C. Full Operational Range Sizing

To ensure that all wind turbines can realize all possible electric operating points within the series string, wind turbine converter ratings can follow a full operational range sizing approach. In this approach, one can consider a wind farm consisting of two series-connected wind turbines (as shown in Fig. 1, assuming $N = 2$). Wind turbine 1 operates at an operating point that puts the wind turbine converter at the maximum of its operational range. Typically, this could refer to the wind turbine converter operating at maximum output voltage while the wind turbine outputs rated power. Wind turbine 2 operates at an operating point that puts the wind turbine converter at the minimum of its operational range. Typically, this could refer to the wind turbine converter operating at minimum output voltage while the wind turbine operates at cut-in wind speed. Converter ratings are then chosen to enable this operating condition. Furthermore, additional constraints related to wind turbine startup or fault handling may need to be observed. Sample realizations of this approach are provided in Sections V and VI.

D. Partial Operational Range Sizing

In certain wind farm configurations, it may happen that the likelihood of operation at or near the full operational range component ratings is very low, or the required component ratings to realize full operational range sizing are considered excessive. In such cases, it can be meaningful to examine the benefits of intentionally reducing converter ratings to only cover a fraction of the full operational range within the wind farm and implement a curtailment scheme for those operational points that are beyond the implemented converter ratings. In addition, full operational range sizing may not prevent violations of the HVdc-link voltage constraint $\overline{V_{\mathrm{HVdc},R}}$. For these cases, a partial operational range sizing approach is discussed next.

As shown in Section II, for all wind turbine operating conditions, there is a range of feasible HVdc-link currents that can be selected. To express the interaction between scheduled HVdc-link current and converter limits, it is meaningful to derive each limit of a particular converter as a function of minimum or maximum possible HVdc-link current. This allows the prediction of violations of converter limits as a function of I_{HVdc} for given wind turbine powers P_n , and informs the choice of HVdc-link current during operation, as well as the prediction of required converter ratings to make an expected operating condition feasible for a particular HVdc-link current.

Within the topology-specific, steady-state relationship of (4), there can be numerous limitations on (internal) state variables or relationships based on (internal) state variables. These limitations can be of static nature, mostly related to component ratings. However, dynamic, $\boldsymbol{S_n}$-dependent limitations can also exist in some converter topologies.

For many of these limitations, the topology-specific relationships of (4) can be solved for I_{HVdc} analytically or numerically, where the limited variable is represented by its rated boundary value or relationship. For instance, for a wind turbine converter with a rated maximum output voltage $\overline{V_{\mathrm{out},R,n}}$, (1) can be reformulated to yield the minimum HVdc-link current, $\underline{I_{\mathrm{HVdc},\overline{V_{\mathrm{out},R,n}}}}$, to avoid exceeding $\overline{V_{\mathrm{out},R,n}}$

$$\underline{I_{\mathrm{HVdc},\overline{V_{\mathrm{out},R,n}}}} = \frac{P_n}{\overline{V_{\mathrm{out},R,n}}} \ . \tag{6}$$

Limits that are not a function of I_{HVdc} indicate that the series-connection of wind turbines has no influence on the determination of that component rating and a traditional sizing approach could be taken. For example, power electronic switches facing the generator might often be chosen to withstand the maximum current that occurs at full-power operation. For this reason, limits that are independent of I_{HVdc} are not discussed further in this article.

E. Limits on HVDC-Link Current

To summarize I_{HVdc}-dependent limits, equations for all converter limits can be formulated from the topology-specific relationship of (4). The $N \times M$ matrix $\underline{\boldsymbol{L}_{\boldsymbol{I}_{\mathbf{HVdc}}}}$ holds minimum HVdc-link current values for all N turbines and all M limits derived previously that result in a lower HVdc-link current limit. Equivalently, the $N \times G$ matrix $\overline{\boldsymbol{L}_{\boldsymbol{I}_{\mathbf{HVdc}}}}$ holds all maximum HVdc-link current values for all N turbines and G limits that result in an upper HVdc-link current limit.

To ensure that the maximum rated HVdc-link voltage $\overline{V_{\mathrm{HVdc},R}}$ is not exceeded under any operating condition, another minimum limit on the HVdc-link current, $\underline{I_{\mathrm{HVdc},\overline{V_{\mathrm{HVdc}}}}}$, must be considered

$$\underline{I_{\mathrm{HVdc},\overline{V_{\mathrm{HVdc}}}}} = \frac{\sum_{n=1}^{N} P_n}{\overline{V_{\mathrm{HVdc},R}}} \ . \tag{7}$$

The overall maximum and minimum allowable HVdc-link currents $\overline{I_{\mathrm{HVdc}}}$ and $\underline{I_{\mathrm{HVdc}}}$ can then be expressed as

$$\overline{I_{\mathrm{HVdc}}} = \min\left(\overline{\boldsymbol{L}_{\boldsymbol{I}_{\mathbf{HVdc}}}}\right) \tag{8}$$

$$\underline{I_{\mathrm{HVdc}}} = \max\left(\begin{bmatrix} \max\left(\underline{\boldsymbol{L}_{\boldsymbol{I}_{\mathbf{HVdc}}}}\right) \\ \underline{I_{\mathrm{HVdc},\overline{V_{\mathrm{HVdc}}}}} \end{bmatrix}\right) . \tag{9}$$

For as long as $\overline{I_{\mathrm{HVdc}}} \geq \underline{I_{\mathrm{HVdc}}}$, I_{HVdc} should be chosen, such that

$$\underline{I_{\mathrm{HVdc}}} \leq I_{\mathrm{HVdc}} \leq \overline{I_{\mathrm{HVdc}}}\,. \tag{10}$$

This ensures that no converter in the wind farm operates at or beyond its limits and no full or partial wind power curtailment is necessary to avoid exceeding converter limits. For such case, HVdc-link current scheduling laws can be used to optimize for objectives not related to converter ratings.

If $\underline{I_{\mathrm{HVdc}}} > \overline{I_{\mathrm{HVdc}}}$, there is no HVdc-link current that can be chosen to maintain all converters operating within their limits. In such case, output power curtailment becomes necessary in one or more wind turbines, to ensure that converter limits are not violated.

F. Sizing Wind Turbine Converters and Incoming Wind Conditions

In the previous section, the converter's state dependence on I_{HVdc} was discussed. However, the converters' states also depend on wind turbine states, such as P_n, $V_{\mathrm{gen},n}$, and f_{gen}, related to the incoming wind conditions, wind turbine control laws, and dynamic response of the aero-mechanic system, respectively.

To eliminate unknowns relating to the incoming wind conditions that will appear in (7) and (9)—such as P_n, $V_{\mathrm{gen},n}$, and f_{gen}—sizing wind turbine converters in series-connected dc wind farms requires a formulation of such wind conditions expected to be present during the operation of such a wind farm for its operational life (e.g., compare with the article presented in [11]).

Provided that a formulation of the expected wind turbine operating conditions and their likelihoods for the life of the wind farm is available, it then becomes possible to predict the likelihood of operating points of wind turbine converters over the life of the wind farm. As a result, it is possible to estimate the likelihood of converters to be operating within their limits and avoiding power curtailment due to converter limits, using relationships (7), (9), and (10). This allows making informed design decisions on the converter ratings and converter topological choices for a series-connected dc offshore wind farm. The proposed key metric during this design process is the expected annual wind energy curtailment due to exceeding converter limits. A flowchart of the proposed sizing framework is provided in Fig. 5. Section VII-A expands on the approach taken to estimate wind turbine operational states for a particular wind farm site.

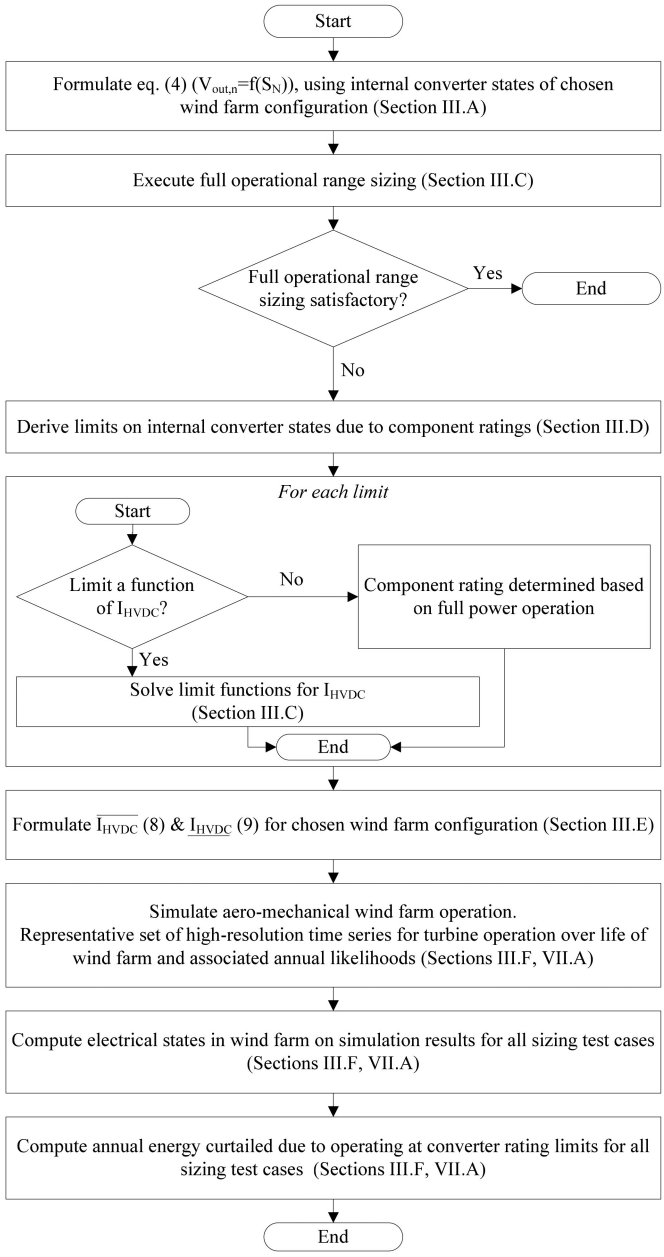

Fig. 5. Flowchart of partial operational range sizing framework for wind turbine converters in single-string, series-connected dc wind farms.

IV. Sizing of a Differential Power Processing Converter-Based Wind Farm

This section discusses the implementation of the partial operating range sizing methodology presented in Section II on a wind farm configuration featuring differential power processing (DPP), as discussed in detail in [14], denominated as "DCS-PPPC" in this article. A full operational range sizing is derived in Section VII for reference purposes. The wind farm configuration is shown in Fig. 6 and its features are summarized next. The series-connected dc wind farm configuration features diode-bridge rectifiers (DBRs) and partial power processing converters (PPPCs) to provide a variable dc output voltage. A current-sourced onshore inverter station controls the link current I_{HVdc}. Finally, a system controller periodically receives selected measurements from each wind turbine, in order to implement an HVdc-link current scheduling scheme and facilitate other system control and management functions.

A. Steady-State System Operation

The wind turbine model and basic controls are based on those of the NREL 5 MW reference wind turbine [39] and are implemented in the SimWindFarm toolbox [40], assuming a medium-voltage generator connected to the rotor using a single-stage

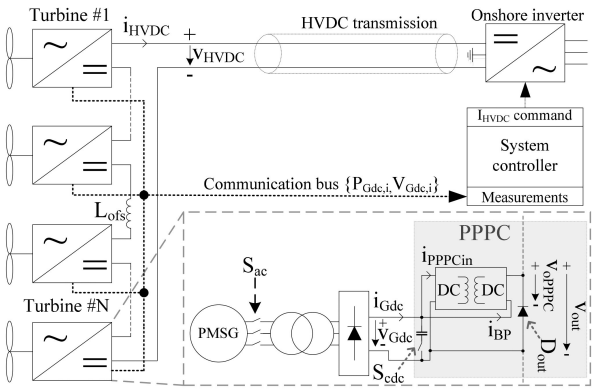

Fig. 6. Structure of a single-string, series-connected dc wind farm featuring PPPCs to realize DPP [2].

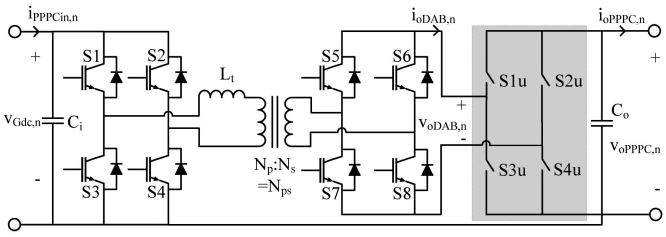

Fig. 7. Dual-active bridge converter and unfolder circuit (in gray) in PPPC.

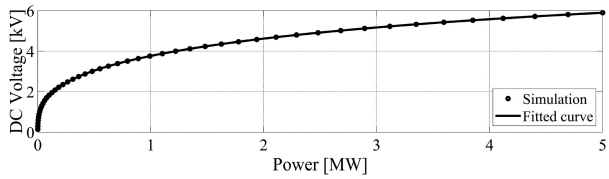

Fig. 8. $V_{Gdc,n}$ versus P_n (simulation and curve fitting of simulation results).

gearbox with a gear ratio $N_{\rm GB}$ of 11.46 (Multibrid drivetrain [41]). The relationship between wind turbine states P_n, $V_{{\rm gen},n}$ and $f_{{\rm gen},n}$, and DBR dc-side average voltage $V_{Gdc,n}$ has been obtained using numerical simulations and is shown in Fig. 8 for the parameters listed in Table I, assuming wind turbine operation at optimal tip-speed ratio between cut-in and rated wind speed. The PPPC terminal average, steady-state relationships are as follows [14]:

$$I_{{\rm PPPC}in,n} = I_{Gdc,n} \; - \; I_{BP,n} = \frac{P_n}{V_{Gdc,n}} \; - I_{{\rm HVdc},n} \tag{11}$$

$$\begin{aligned} P_{{\rm PPPC},n} &= V_{Gdc,n} \;\; I_{{\rm PPPC}in,n} = V_{Gdc,n} \;\; (I_{Gdc,n} - I_{\rm HVdc}) \\ &= P_n - V_{Gdc,n} {\rm I}_{{\rm HV}dc} \end{aligned} \tag{12}$$

$$V_{o{\rm PPPC},n} = \frac{P_{{\rm PPPC},n}}{I_{\rm HVdc}} \; = \frac{P_n}{I_{\rm HVdc}} \; - V_{Gdc,n} \tag{13}$$

$$V_{{\rm out},n} = V_{o{\rm PPPC},n} \; + \; V_{Gdc,n} = V_{Gdc,n} \, \frac{I_{Gdc,n}}{I_{\rm HVdc}} \tag{14}$$

where all electrical quantities follow the definitions in Fig. 6.

TABLE I
WIND FARM PARAMETERS

WIND TURBINE, GENERATOR		RATED / BASE VALUES	
Rated power	5 MW	5 MW, 5.8 kV, 862 A	
Cut-in wind speed	3.5 m/s	DAB CONVERTER (ALL TEST CASES)	
Rated wind speed	11.25 m/s	Turns ratio N_{ps}	2
Rated rotor speed	1.357 rad/s	Switching frequency	7500 Hz
Gearbox ratio	1:11.46	Capacitor C_o	540 µF
Pole-pair count	14	Input voltage rating	6500 V *
Rated voltage	5 kV	Output current rating	2864 A
Synch. inductance	7.5 mH	HVDC SYSTEM	
For other parameters, see [13]		Cable length	100 km
		Rated HVDC voltage	± 113 kV

*This includes the required safety margin for the IGBTs.

The PPPC is realized as a dual-active bridge (DAB) converter, as shown in Fig. 7. Here, a single phase-shift (SPS) modulation scheme is considered. For simplicity reasons, no multiconverter realization is considered, unlike in [14]. The output power for the DAB converter with SPS modulation scheme is a function of its terminal voltages $V_{Gdc,n}$ and $V_{o{\rm DAB},n}$, and phase shift ϕ [42]

$$P_{{\rm PPPC},n} = \frac{V_{Gdc,n} V_{o{\rm DAB},n} N_{ps}}{2\pi f_s L_t} \; \phi_n \left(1 - \frac{|\phi_n|}{\pi}\right) \tag{15}$$

where N_{ps} and L_t are the transformer's turns ratio and leakage inductance, as defined in Fig. 7; f_s is the converter switching frequency and ϕ_n the phase shift. To enable bidirectional power transfer for the DAB with bipolar voltage $V_{o{\rm PPPC},n}$, but unipolar current $I_{\rm HVdc}$, an unfolder circuit composed of switches S1u–S4u in Fig. 7 has been added. When $V_{o{\rm PPPC},n}$ is positive, S1u and S4u are closed, and when $V_{o{\rm PPPC},n}$ is negative, S2u and S3u are closed to maintain a positive $V_{o{\rm DAB},n}$, but negative $i_{o{\rm DAB},n}$. For zero $V_{o{\rm PPPC},n}$, all unfolder switches are closed to bypass the DAB. As a result, the unfolder terminal characteristics are given as [14]

$$V_{o{\rm PPPC},n} = \; UF_n \times V_{o{\rm DAB},n} \; ; V_{o{\rm DAB},n} \geq 0 \tag{16}$$

$$I_{o{\rm DAB},n} = \; UF_n \times I_{\rm HVdc}; \; I_{\rm HVdc} \geq 0 \tag{17}$$

where UF_n is the unfolder polarity, defined as ${\rm sign}(P_{{\rm PPPC},n})$, and all other quantities are defined in Fig. 6.

In summary, the topology-specific, steady-state relationship of (4) for this wind farm configuration consists of the numerical relationship $V_{Gdc,n} = \; f(P_n, V_{{\rm gen},n}, f_{{\rm gen},n})$ of Fig. 8, and (13)–(16) to obtain a relationship for $V_{{\rm out},n}$ involving internal DBR and PPPC states

$$V_{{\rm out},n} = \frac{V_{Gdc,n} V_{o{\rm DAB},n} N_{ps}}{2\pi f_s L_t I_{\rm HVdc}} \; \phi_n \left(1 - \frac{|\phi_n|}{\pi}\right) + V_{Gdc,n}. \tag{18}$$

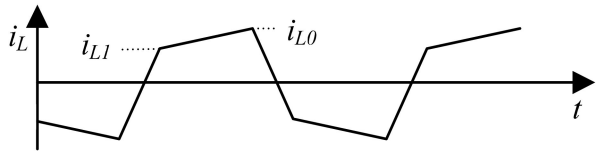

Fig. 9. Definition of DAB transformer current points i_{L0} and i_{L1}.

B. I_{HVDC}-Dependent Converter Limits

As discussed in Section III-C, converter limits that are not a function of I_{HVdc} would lead to a conventional sizing approach and are neglected in this analysis. In particular, this relates to the DBR diodes' voltage and current ratings, as well as the voltage rating of the primary DAB switches S1–S4.

Component ratings depending on I_{HVdc} that are derived from converter limits in this wind farm configuration are as follows:

1) current rating of all DAB switches;
2) voltage rating of switches S5–S8 and S1u–S4u;
3) DAB leakage inductance L_t and switching frequency f_s, related to maximum PPPC power capability.

The converter limits that need to be considered in relation to these component ratings are on the following:

1) DAB output voltage $V_{o\mathrm{PPPC},n}$: $\overline{V_{o\mathrm{PPPC},n}}$ and $\underline{V_{o\mathrm{PPPC},n}}$;
2) peak current of DAB transformer current $i_{L,n}$: $\overline{|i_{L,pk,n}|}$;
3) maximum and minimum DAB power (related to maximum and minimum DAB phase shift ϕ): $\overline{P_{\mathrm{PPPC},n}}$ and $\underline{P_{\mathrm{PPPC},n}}$.

C. PPPC Output Voltage Limits

The maximum and minimum output voltage of the PPPC is determined by the voltage ratings of switches S5–S8 and S1u–S4u. From (13), the HVdc-link current can be related to the PPPC output voltage

$$I_{\mathrm{HVdc}} = \frac{P_n}{V_{o\mathrm{PPPC},n} + V_{Gdc,n}}\,. \tag{19}$$

As a result, to not violate the maximum and minimum PPPC output voltage limits, the minimum and maximum HVdc-link current values are defined as

$$\frac{P_n}{\overline{V_{o\mathrm{PPPC},n}} + V_{Gdc,n}} < I_{\mathrm{HVdc}} < \frac{P_n}{\underline{V_{o\mathrm{PPPC},n}} + V_{Gdc,n}}. \tag{20}$$

D. Internal DAB Current Limit

To determine the DAB switch current ratings, as well as DAB switching frequency and leakage inductance, it is necessary to determine the DAB transformer peak current. The peak current $i_{L,pk,n}$ in a DAB inductor L_t is

$$i_{L,pk,n} = \max\left(|i_{L0,n}|\ |i_{L1,n}|\right)\ \frac{V_{Gdc,n}}{2\pi f_s L_t} \tag{21}$$

where $i_{L0,n}$ and $i_{L1,n}$ mark characteristic saddle or extremum points in the inductor current waveform, as shown in Fig. 9, and f_s is the DAB switching frequency. According to [42], these points can be calculated for SPS modulation as follows:

$$i_{L0,n} = \begin{cases} \frac{(1+m_n)\phi_n}{2} + \frac{(1-m_n)(\pi-\phi_n)}{2}, & \phi_n > 0 \\ 0.5\left[-2m_n\phi_n + (1-m_n)\,\pi\right], & \phi_n < 0 \wedge m_n < 1 \\ 0.5\left[-(m_n-1)\,\pi\right], & \phi_n < 0 \wedge m_n > 1 \end{cases} \tag{22}$$

$$i_{L1,n} = \begin{cases} \frac{(1+m_n)\phi_n}{2} - \frac{(1-m_n)(\pi-\phi_n)}{2}, & \phi_n > 0 \\ 0.5\left[-(m_n-1)\,\pi\right], & \phi_n < 0 \wedge m_n < 1 \\ 0.5\left[2\phi_n - (m_n-1)\,\pi\right], & \phi_n < 0 \wedge m_n > 1. \end{cases} \tag{23}$$

In (22) and (23), $m_n = N_{ps}\ V_{o\mathrm{DAB},n}/V_{Gdc,n}$ and ϕ_n is the phase shift in radians of the SPS modulation. The maximum absolute DAB power is reached with ϕ_n equal to $\pm\frac{\pi}{2}$. Using (13), m_n is rewritten as

$$m_n = N_{ps}\ \left(P_n/\ I_{\mathrm{HVdc}} - 1\right). \tag{24}$$

ϕ_n can be determined numerically for a particular operating condition using (12) and (15). Using (21)–(24), it then becomes possible to numerically determine the peak currents in the DABs primary and secondary switches S1–S8 as a function of P_n, $V_{Gdc,n}$ and I_{HVdc}, as well as converter parameters

$$i_{L,pk,n} = g\left(P_n, V_{Gdc,n}, I_{\mathrm{HVdc}}\right). \tag{25}$$

Conversely, (25) can also be solved numerically for I_{HVdc} as a function of $i_{L,pk,n}$, P_n and $V_{Gdc,n}$. To ensure that the resulting function has unique solutions, it is done for $P_{\mathrm{PPPC}.n} \geq 0$ and $P_{\mathrm{PPPC},n} < 0$ separately. For $P_{PPPC,n} \geq 0$

$$I_{\mathrm{HVdc}} = k^{+}\ \left(P_n, V_{Gdc,n}, i_{L,pk,n}\right). \tag{26}$$

Similarly, for $P_{\mathrm{PPPC},n} < 0$

$$I_{\mathrm{HVdc}} = k^{-}\ \left(P_n, V_{Gdc,n}, i_{L,pk,n}\right). \tag{27}$$

This separation is necessary since $i_{L,pk,n}$ is monotonically increasing as $|P_{PPPC,n}|$ increases, yielding two solutions for I_{HVdc} for many operating points without such separation.

E. DAB Power Limit

The DAB phase shift ϕ_n is bound within the range of $-\pi/2$ to $\pi/2$. At the two extremes, the DAB processes the minimum and maximum possible amounts of power, respectively [42]. Using (13) and (16), (15) can be rewritten to

$$I_{\mathrm{HVdc}} = \frac{V_{Gdc,n}N_{ps}}{UF_n \times 2\pi f_s L_t}\ \phi_n\left(1 - \frac{|\phi_n|}{\pi}\right). \tag{28}$$

Since the unfolder polarity UF_n is defined as $sign\ \left(P_{\mathrm{PPPC},n}\right) = \ \mathrm{sign}(\phi_n)$, (28) resolves to the same solution for $\phi_n = \ \pi/2$ and $\phi_n = \ -\pi/2$. An upper limit to the HVdc-link current results to maintain stable DAB operation within its power limits

$$I_{\mathrm{HVdc}} < V_{Gdc,n}N_{ps}/8f_sL_t. \tag{29}$$

F. Wind Turbine Startup and Shutdown

The scheme presented in [37] demonstrates a wind turbine startup and shutdown procedure that does not significantly affect converter sizing. For this reason, wind turbine startup and shutdown is not considered further in this analysis.

G. Fault Ride Through

As shown in [14], low-voltage ride-through (LVRT) is handled using an onshore braking chopper that maintains the operating conditions of the offshore wind farm during an LVRT event. Therefore, LVRT does not influence converter sizing for this wind farm configuration.

H. Fault Handling

It is assumed that wind turbine internal faults in a single-string, series-connected wind farm can be handled by de-energizing and bypassing a wind turbine in the string. Faults in the collection system could be handled by adopting fault handling schemes, such as those discussed in [38], which show that faults can be handled without affecting the PPPC input current or output voltage ratings, and allow clearing a ground fault with an HVdc-link current peak of approximately 2.5 p.u. For this reason, a minimum peak output current rating constraint of 2.5 p.u. is considered here.

I. Internal Wind Turbine States $\boldsymbol{S_{I,n}}$

Using the steady-state relationship between $V_{Gdc,n}$ and P_n provided in Fig. 8, all steady-state average quantities in (11)–(17) can be computed. Additionally, for the purpose of evaluating component limits, it is necessary to determine the DAB peak current $i_{L,pk,n}$ following (21)–(24). As a result, the internal state vector $\boldsymbol{S_{I,n}}$ is defined as

$$\boldsymbol{S_{I,n}} = \left[V_{Gdc,n} \; i_{L,pk,n} \right]^{\boldsymbol{T}}. \tag{30}$$

J. Allowable HVDC-link Currents

In summary, the maximum and minimum allowable HVdc-link currents $\underline{I_{\mathrm{HVdc}}}$ and $\overline{I_{\mathrm{HVdc}}}$ are derived and written in matrix form, as discussed in Section III-C

$$\underline{\boldsymbol{L_{I_{\mathbf{HVdc}}}}} = \begin{bmatrix} P_n / \left(V_{Gdc,n} + \overline{V_{o\mathrm{PPPC}}} \right) \\ k^{+} \left(P_n, V_{Gdc,n}, i_{L,pk,n} = \overline{I_{S1-S4}} \right) \\ k^{+} \left(P_n, V_{Gdc,n}, i_{L,pk,n} = \frac{\overline{I_{S5-S8}}}{N_{ps}} \right) \end{bmatrix} \tag{31}$$

$$\overline{\boldsymbol{L_{I_{\mathbf{HVdc}}}}} = \begin{bmatrix} P_n / \left(V_{Gdc,n} + \underline{V_{o\mathrm{PPPC}}} \right) \\ k^{-} \left(P_n, V_{Gdc,n}, i_{L,pk,n} = \underline{I_{S1-S4}} \right) \\ k^{-} \left(P_n, V_{Gdc,n}, i_{L,pk,n} = \frac{\underline{I_{S5-S8}}}{N_{ps}} \right) \\ V_{Gdc,n} N_{ps} / 8 f_s L_t \end{bmatrix} \tag{32}$$

where in $\underline{\boldsymbol{L_{I_{\mathbf{HVdc}}}}}$ and $\overline{\boldsymbol{L_{I_{\mathbf{HVdc}}}}}$ the rows represent the PPPC output voltage limit, primary bridge DAB peak current limit, and secondary bridge DAB peak current limit, respectively. The last row of $\overline{\boldsymbol{L_{I_{\mathbf{HVdc}}}}}$ represents the maximum DAB power limit.

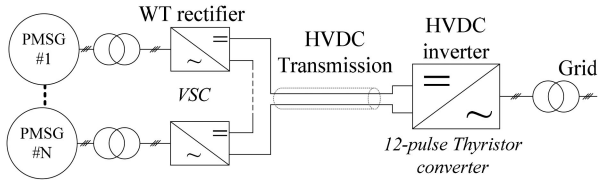

Fig. 10. Structure of the DCS-VSC configuration.

The minimum and maximum allowable HVdc link currents for this wind farm configuration can then be determined following (7)–(9).

V. Sizing of a Voltage-Source Converter-Based Wind Farm

This section implements the sizing methodology for a VSC-based wind farm, as discussed in [43], adapted to a single-string configuration from [22] and denominated as "DCS-VSC". In this wind farm configuration, VSCs are used as wind turbine converters, as shown in Fig. 10. All other wind farm components are identical to those of the DCS-PPPC configuration. The wind turbine output voltage is given by [44] as

$$V_{\mathrm{out},n} = \frac{2\sqrt{2}}{\sqrt{3}} \frac{V_{\mathrm{gen},n}}{m_a} \tag{33}$$

where $V_{\mathrm{gen},n}$ is the generator line-to-line rms voltage and m_a the modulation index. To maintain linear PWM modulation, the modulation index is assumed to be equal or less than one. As a result it is required that

$$V_{\mathrm{out},n} \geq \frac{2\sqrt{2}}{\sqrt{3}} V_{\mathrm{gen},n}. \tag{34}$$

The HVdc-link current is determined such that each wind turbine operates with a feasible output voltage in addition to a margin k (e.g., 110%) for control action

$$I_{\mathrm{HVdc}} = \frac{P_n}{\max\limits_{1 \leq n \leq N} k \frac{2\sqrt{2}}{\sqrt{3}} V_{\mathrm{gen},n}}. \tag{35}$$

The VSC's switch current ratings are determined from rated ac currents, which are not a function of I_{HVdc}.

A. Full Operational Range Sizing

Considering the wind turbine converter output voltages of a two-turbine series string operating at extreme operating points, one can write

$$V_{\mathrm{out},1} = \frac{P_{\mathrm{rated}}}{I_{\mathrm{HVdc}}} \tag{36}$$

$$V_{\mathrm{out},2} = \frac{P_{\mathrm{min}}}{I_{\mathrm{HVdc}}} \tag{37}$$

where $V_{\mathrm{out},1}$ and $V_{\mathrm{out},2}$ are the converter output voltages of wind turbine 1 and 2, respectively, and P_{rated} and P_{min} are the wind turbine powers at rated and cut-in wind speeds. Using (34), (36), and (37) can be rewritten as (38) and (39) to yield conditions for

feasible values for I_{HVdc}

$$I_{\mathrm{HVdc}} \leq \frac{P_{\mathrm{rated}}}{k\frac{2\sqrt{2}}{\sqrt{3}}V_{\mathrm{gen,rated}}} \tag{38}$$

$$I_{\mathrm{HVdc}} \leq \frac{P_{\mathrm{min}}}{k\frac{2\sqrt{2}}{\sqrt{3}}V_{\mathrm{gen,min}}} \tag{39}$$

where $V_{\mathrm{gen,rated}}$ and $V_{\mathrm{gen,min}}$ are the generator voltages at rated and cut-in operating conditions, respectively.

Numerical analysis of (38) and (39) for a wind turbine design presented in Section VII reveals that condition (39) is tighter for the entire output power range. Using (39), solving (1) for I_{HVdc} and considering rated converter output voltage $V_{\mathrm{out,rated}}$ lead to

$$V_{\mathrm{out,rated}} \geq \frac{2\sqrt{2}k}{\sqrt{3}}V_{\mathrm{gen,min}}\frac{P_{\mathrm{rated}}}{P_{\mathrm{min}}}. \tag{40}$$

For the presented wind turbine parameters, the rated output voltage would need to be at least 61.2 kV for a 3300 V generator, assuming k equal to 1.1, $\frac{P_{\mathrm{rated}}}{P_{\mathrm{min}}}$ equal to 33.21 and $V_{\mathrm{gen,min}}$ equal to 1129 V.

B. Partial Operational Range Sizing

Given the very high required output voltage rating for full operational range sizing, partial operational range sizing appears worth exploring. Given the converter output voltage constraint of (34), the maximum HVdc-link current constraint due to this output voltage constraint $\overline{I_{\mathrm{HVdc},\underline{V_{\mathrm{out},R,n}}}}$, can be written as

$$\overline{I_{\mathrm{HVdc},\underline{V_{\mathrm{out},R,n}}}} = \frac{P_n}{\frac{2\sqrt{2}}{\sqrt{3}}V_{\mathrm{gen},n}}\ . \tag{41}$$

As a result, the maximum and minimum allowable HVdc-link currents $\underline{I_{\mathrm{HVdc}}}$ and $\overline{I_{\mathrm{HVdc}}}$ are derived and written in matrix form, as discussed in Section III-C

$$\underline{\boldsymbol{L}_{\boldsymbol{I_{\mathbf{HVdc}}}}} = [0] \tag{42}$$

$$\overline{\boldsymbol{L}_{\boldsymbol{I_{\mathbf{HVdc}}}}} = \left[\ \frac{P_n}{\frac{2\sqrt{2}}{\sqrt{3}}V_{\mathrm{gen},n}}\ \right]\ . \tag{43}$$

The overall minimum and maximum allowable HVdc link currents for this wind farm configuration can then be determined following (7)–(9).

1) Wind Turbine Startup and Shutdown: Wind turbine startup of this wind farm configuration may face challenges similar to those reported in [37]. For the purpose of this article, it is assumed that additional hardware and/or control algorithms are used to facilitate wind turbine startup that do not result in further sizing constraints on the VSC.

2) Fault Ride-Through and Fault Handling: Fault ride-through can be handled in the same way, as discussed in Section IV-G. Similarly, it is assumed that fault handling is realized in a way similar to that discussed in Section IV-H. However, VSC switch current ratings may not already be sufficient and may require an increased rating to withstand a 2.5 p.u. current peak during ground faults, as discussed in [38].

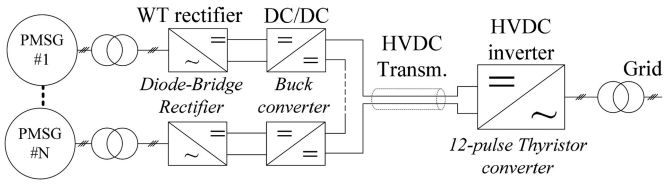

Fig. 11. Structure of the DCS-buck configuration.

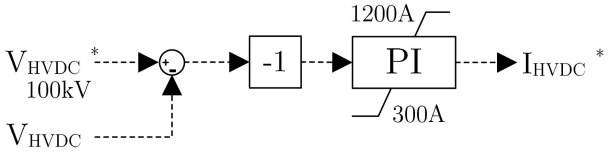

Fig. 12. HVdc-link current scheduling scheme of [13].

VI. Sizing of a Farm Based on Diode-Bridge Rectifier and Buck Converter

Finally, the sizing of a wind farm configuration featuring diode-bridge rectifiers and buck converters [13] is discussed in this section. This configuration is labelled as "DCS-buck" and shown in Fig. 11. All components are identical to those of DCS-PPPC, aside from the wind turbine converter. The HVdc-link current scheduling scheme of [13] is shown in Fig. 12. Due to the buck converter, the wind turbine output voltage must be less than or equal to the diode-bridge rectifier's dc-side voltage $V_{Gdc,n}$

$$V_{\mathrm{out},n} \leq\ V_{Gdc,n}. \tag{44}$$

$V_{Gdc,n}$ as a function of P_n has been derived in Section IV-A and is shown in Fig. 8.

A. Full Operational Range Sizing

Considering the wind turbine converter output voltages of a two-turbine series string operating at extreme operating points, one can write

$$V_{\mathrm{out},1} = \frac{P_{\mathrm{rated}}}{I_{\mathrm{HVdc}}} \tag{45}$$

$$V_{\mathrm{out},2} = \frac{P_{\mathrm{min}}}{I_{\mathrm{HVdc}}} \tag{46}$$

where $V_{\mathrm{out},1}$ and $V_{\mathrm{out},2}$ are the converter output voltages of wind turbines 1 and 2, respectively, and P_{rated} and P_{min} are the wind turbine powers at rated and cut-in wind speed. Using (44), (45), and (46) can be rewritten as (47) and (48) to yield conditions for feasible values for I_{HVdc}

$$I_{\mathrm{HVdc}} \geq \frac{P_{\mathrm{rated}}}{V_{Gdc,n}\left(P_{\mathrm{rated}}\right)} \tag{47}$$

$$I_{\mathrm{HVdc}} \geq \frac{P_{\mathrm{min}}}{V_{Gdc,n}\left(P_{\mathrm{min}}\right)}\ . \tag{48}$$

Numerical analysis of (47) and (48) for a wind turbine design presented in Section VII reveals that condition (47) is tighter for

the entire output power range. Using (47), solving (1) for I_{HVdc} and considering rated converter output voltage $V_{\mathrm{out,rated}}$ lead to

$$V_{\mathrm{out,rated}} \geq V_{Gdc,n}\left(P_{\mathrm{rated}}\right). \tag{49}$$

For the presented wind turbine parameters, the rated output voltage would need to be at least 5.8 kV for a 5000 V generator, and the required output current rating would be 862 A, neglecting fault handling related issues. Veilleux and Lehn [13] chose an output voltage and current rating of 4166 V and 1200 A. In this design, the buck converter semiconductors still require a voltage rating of 5.8 kV to withstand the maximum V_{Gdc} value, but require a higher current rating for an average output current of 1200 A.

Since operation at rated output values represents the only feasible operating point in this configuration to process rated power, the consideration of partial operational range sizing is not meaningful with the DCS-Buck configuration to reduce component sizes.

B. Wind Turbine Startup and Shutdown

Due to the buck converter's ability to operate with zero output voltage and power, wind turbine startup of this wind farm configuration is expected to be similar to those of conventional schemes and without further implications on converter ratings.

C. Fault Ride-Through and Fault Handling

Fault ride-through can be handled in the same way as discussed in Section IV-G. Fault handling for this wind farm configuration has been studied in [29] and it is indicated that a peak current rating for short durations of 2 p.u. may be required to contain dc link faults.

VII. Converter Sizing Case Studies for a 450 MW Offshore Wind Farm

To demonstrate the efficacy of the sizing methodology, three case studies for a 450 MW Offshore Wind Farm are discussed in this section. The fictional wind farm under consideration consists of 90 5 MW wind turbines located near the FINO3 meteorological mast site in the North Sea, 80 km off the coasts of Denmark and Germany. The wind farm consists of three subfarms, each operating 30 wind turbines with separate electrical systems that are interconnected at the onshore inverter stations' ac side [14]. The wind farm layout is shown in Fig. 13 and key wind farm parameters are given in Table I. The first case study considers sizing such a wind farm with the DCS-PPPC configuration. A second study considers the DCS-VSC, followed by a last study on the DCS-buck configuration.

A. Determination of Wind Turbine Operational States and Energy Curtailment

To predict expected wind turbine and wind farm states, 7 years of 10-min-resolution wind measurements of the FINO3 met mast (average rotor equivalent wind speed, wind direction, and turbulence intensity) were binned into 7508 unique wind conditions and the likelihood of occurrence for each bin was recorded. The

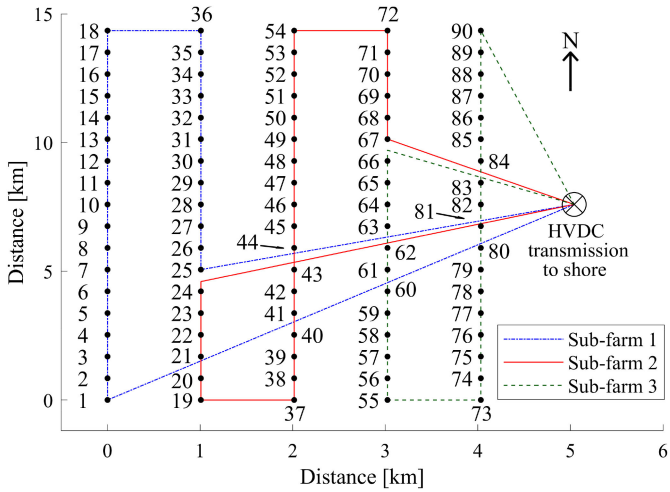

Fig. 13. Wind farm layout and collection system for subfarms 1–3.

bin sizes are 1 m/s, 10°, and 1% for wind speed, direction, and turbulence intensity, respectively. For each of these 7508 wind conditions, the entire wind farm was simulated using the SimWindFarm toolbox available for MATLAB/Simulink [40]. This toolbox realizes time-transient, dynamic simulations of aerodynamic-mechanical systems of wind turbines in a wind farm, taking into account upwind wind speed, wind direction, turbulence intensity, and wake effects. For each of the 7508 simulation runs, the wind turbine output power, rotational speed, and rotor-equivalent wind speeds were recorded with a 1-s time resolution for a duration of a wind field passing the wind farm twice at any given average wind speed. These simulations were executed on a heterogeneous computational cluster (Compute Canada, Cedar) due to large computational and memory requirements of such a simulation.

It was assumed that electrical transients are significantly faster than the 1-s time step, such that near steady-state operation can be assumed for all electrical systems with respect to the chosen time step. The time series of wind turbine power, rotational speed and wind speed simulation were then used to compute the operational states of the electric wind farm components using their steady-state models, as discussed in the following paragraphs specific to each wind farm configuration.

Finally, the average amount of energy curtailed per second due to converter limits was computed for each of the 7508 simulations. This average energy curtailment per case was then weighed by the likelihood of occurrence of each of the 7508 cases, as recorded by the FINO3 met mast. The final amount of energy curtailment is then obtained as

$$E_{\mathrm{curt,year}} = \sum_{n=1}^{7508} P_{\mathrm{curt}}\left[n\right] \times \phi\left[n\right] \times \left(60 \times 60 \times 24 \times 365\right) \frac{s}{a} \tag{50}$$

where $E_{\mathrm{curt,year}}$ is the expected amount of energy curtailed per year due to converter limits, the index number n denoting each of the 7508 cases observed by the FINO3 met mast, $P_{\mathrm{curt}}[n]$ the average energy curtailed per second for case n, and $\phi[n]$ he

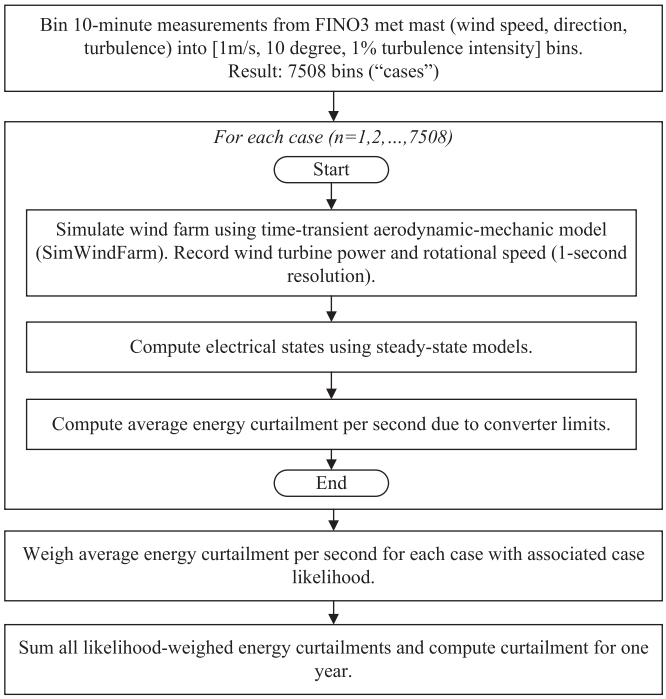

Fig. 14. Determination of wind turbine operational states and energy curtailment for 450 MW wind farm sizing case studies.

TABLE II
DAB CONVERTER TEST CASES

TEST CASE	LEAKAGE INDUCTANCE L_t	OUTPUT VOLTAGE RATING	INPUT CURRENT RATING
1	$740\mu H$	$1247\ V = 0.22\ pu$	$336\ A = 0.39\ pu$
2	$592\mu H$	$1558\ V = 0.27\ pu$	$419\ A = 0.49\ pu$
3	$493\mu H$	$1870\ V = 0.32\ pu$	$503\ A = 0.58\ pu$
4	$423\mu H$	$2181\ V = 0.38\ pu$	$587\ A = 0.68\ pu$
5	$370\mu H$	$2493\ V = 0.43\ pu$	$671\ A = 0.77\ pu$
6	$247\mu H$	$3739\ V = 0.65\ pu$	$1007\ A = 1.17\ pu$
7	$185\mu H$	$4986\ V = 0.86\ pu$	$1342\ A = 1.56\ pu$
8	$118\mu H$	$5800\ V = 1.00\ pu$	$2097\ A = 2.43\ pu$

associated likelihood of occurrence of case n. This workflow is depicted in Fig. 14.

For the DCS-PPPC configuration, electrical converter states were calculated based on relations in Section IV-A and [14]. To study different converter sizing options, eight candidate converter ratings have been applied to the calculation of converter operating conditions, as shown in Table II and visualized in Fig. 15. Test cases 1–7 represent a partial operating range sizing, as there is no valid HVdc-link current to realize unconstrained converter operation at cut-in and rated output power simultaneously. Test case 8 represents a full operational range sizing, as an HVdc-link current of approximately 0.5 p.u. allows an unconstrained operation of converters at full and cut-in wind turbine power, as shown in Fig. 15.

Converter operating conditions for the DCS-VSC configuration have been calculated based on relations given in Section V and [11]. Seven test cases have been considered for this configuration to assess potential benefits from a partial operational

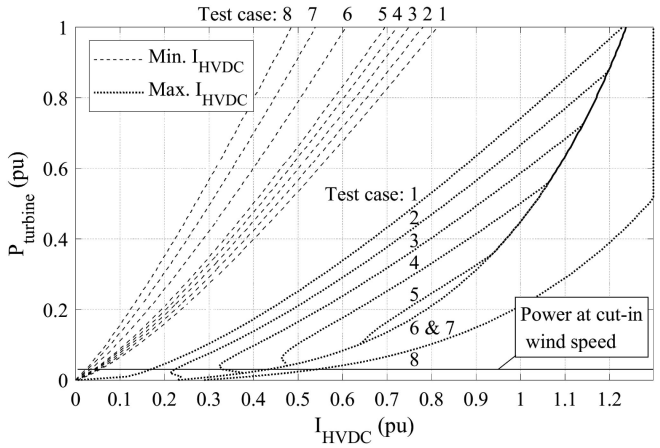

Fig. 15. Possible wind turbine operating points without PPPC sizing-related power curtailment for different HVdc-link currents and all eight DCS-PPPC test cases.

range sizing, compared to a full operational range sizing that is represented by an eighth test case. VSC output voltage ratings are set to multiples of 9 kV, up to 63 kV. It is worth noting that a VSC with a 63 kV output voltage rating can be challenging to implement given limited IGBT output voltage ratings available. Such high output voltage rating is analyzed mainly to outline the trends on energy curtailment with sizing up to full operational range sizing.

For the DCS-buck configuration, diode-bridge rectifier states were derived using the relations depicted in Fig. 8. Remaining states were calculated using relations discussed in Section VI and [29]. As partial operational range sizing has been found infeasible for this configuration, two test cases based on full operational range sizing are evaluated to confirm that no energy curtailment is to be expected from these sizing choices. The first test case is based on the converter output ratings originally discussed in [29] (4166 V and 1200 A), whereas the second test case examines the converter output ratings suggested in Section VI (5800 V and 862 A).

To preserve the general trends of this analysis, component ratings have not been matched with commonly available device ratings. In a final design iteration, these and desired safety margins should be considered.

It has been assumed that wind turbine operation at or beyond converter limits results in a partial or full wind power curtailment: a wind turbine converter operating at maximum limits curtails the wind turbine power to the maximum that can be processed with the converter at its current limit, while pitch control ensures proper speed control of the turbine; a converter operating beyond minimum limits results in the wind turbine coming to a stand-still, as the converter cannot reduce the (inherent) DBRs natural power draw at a given HVdc-link current sufficiently to restore a balance of power between incoming wind power and electric power absorption. It is worth noting that the minimum limit does not apply to the DCS-buck configuration, as the buck converter is capable of operating down to and at zero output voltage and power at any operating condition. The HVdc-link

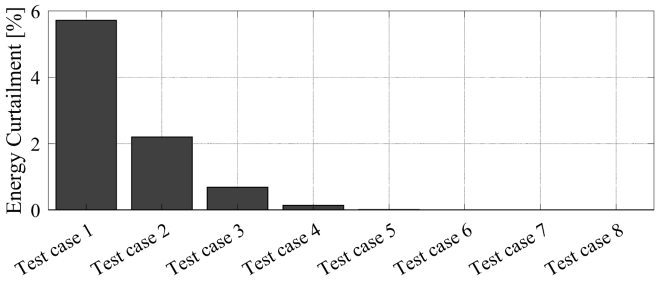

Fig. 16. Estimated annual energy curtailment of DCS-PPPC configuration as percentage of annual energy production due to PPPC component rating limitations.

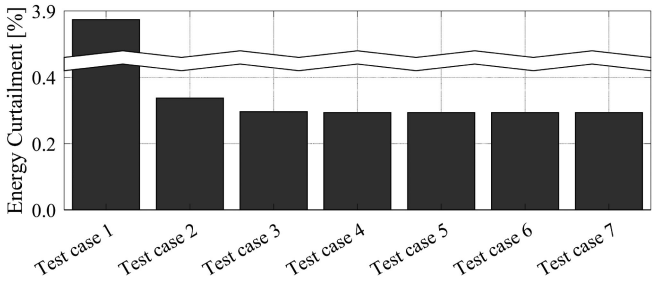

Fig. 17. Estimated annual energy curtailment of DCS-VSC configuration as percentage of annual energy production due to converter component rating limitations.

current was scheduled in such a way to minimize the occurrence of curtailment action using relations (31), (32), (43), and (47), respectively.

Based on this analysis, the amount of annual energy curtailment due to the converters operating at their limits can be predicted. This is used to inform the sizing of such converters.

B. Results – DCS-PPPC

The annual energy curtailment due to exceeding converter limitations has been estimated using the simulations outlined in the previous section. As can be seen in Fig. 16, there is a significant difference in annual energy curtailment due to wind turbine converter sizing decisions. If the PPPCs are rated for 0.22 p.u. output voltage rating (test case 1), more than 5% of potential annual energy production is lost due to curtailment. As PPPC ratings increase, less energy curtailment is necessary. For a PPPC output voltage rating of 0.38 p.u. and input current rating of 0.68 p.u., only 0.13% of annual energy production potential is curtailed (test case 4). A further increase of PPPC ratings decreases the need for curtailment only marginally. Numerical results indicate the presence of a negligible amount of energy curtailment for test cases 5, 6, and 7 ($<$0.01%). The full operational range sizing case (test case 8) results confirms that the wind farm could operate without energy curtailment due to converter limits. However, it is expected that the increase in switch ratings will contribute negatively to converter losses and capital cost of wind turbines, compared to partial operational range sizing test cases (such as test cases 4 and 5, for example). In particular, it requires 2.6 times the PPPC output voltage and 3.6 times the PPPC input current rating compared to test case 4.

This demonstrates how the presented PPPC sizing methodology can be applied to inform decisions about component ratings for power converters for wind farms with single-string series-connected dc collection systems.

Based on these results, it appears reasonable to consider converter ratings similar to those of test case 4 or 5 as there is only a negligible decrease in annual energy production to be expected. Based on local electricity market conditions, an economic assessment between converter cost and value of curtailed energy due to converter rating limitations can further solidify the choice of converter ratings.

C. Results – DCS-VSC

The expected annual energy curtailment due to converter limits has also been estimated for the DCS-VSC configuration. The results are shown in Fig. 17. As can be seen, a VSC with output voltage rating of 9 kV (test case 1) results in approximately 3.9% of available energy to be curtailed due to converter limits. However, VSC output voltage ratings of 18 kV and higher only result in approximately 0.3% of annual energy production to be curtailed. For test cases 3 to 7, most energy curtailment stems from preventing excessive HVdc-link voltages. There are several design aspects in series-connected dc wind farms to be considered, such as maximum possible insulation to ground (i.e., maximum HVdc-link voltage) [14] and system design for high conversion efficiencies [43]. It may be possible to optimize the system to reduce or eliminate the HVdc-link voltage rating-related curtailment. Ultimately, an economic assessment might be useful to find the lowest-cost design tradeoff between rated HVdc-link voltages, wind turbine voltage levels, number of wind turbines per string and conversion losses—all of which are factors that can relate to the amount of energy curtailment due to excessive HVdc-link voltages or stem from measures addressing these.

D. Results – DCS-Buck

Following the methodology discussed in Section VII-A, annual energy curtailment has been estimated for the DCS-buck configuration. Since both test cases followed the full operational range sizing approach, no energy curtailment due to converter limits was expected. The simulation of both test cases confirmed that there is no energy curtailment due to converter limits to be expected. The second test case examining converter output ratings suggested in Section VI (5800 V and 862 A) resulted in overall higher HVdc-link voltages and lower HVdc-link currents. This indicates that there is a potential for efficiency improvements in the collection and transmission systems through current reduction on an annual average compared to the sizing initially suggested in [29].

VIII. Conclusion

In this article, a methodology for determining the component ratings of wind turbine converters in single-string, series-connected dc wind farms has been developed. As demonstrated in this article, the series connection of wind turbines with dc output results in a strong interdependence of operating points among the wind turbines in a wind farm. Consequently, traditional methods of sizing wind turbine converters are not useful for determining all component voltage and current ratings in these kinds of wind farms. First, this article presents a generic sizing framework, applicable to all single-string, series-connected dc wind farms. A distinction between full and partial operational range sizing approaches is made. It then applies the analytical framework to a wind farm configurations featuring differential power processing, voltage-source converters, and diode-bridge rectifiers and buck converters. The main design consideration in this sizing methodology is the reduction of energy curtailment resulting from finite component ratings while minimizing component ratings to partial operational range sizing. Finally, a case study for a 450 MW wind farm demonstrates the implementation of the proposed sizing methodology and shows that converter output voltage rating of about 0.38 p.u. and input current ratings of 0.68 p.u. are sufficient for a proper wind farm operation for the wind farm configuration featuring differential power processing, with negligible energy curtailment due to finite converter ratings, and avoiding extra installation costs due to oversizing. Similarly, a voltage-source converter-based wind farm configuration may operate with low energy curtailment using converters rated at 18 kV or higher. The wind farm configuration featuring diode-bridge rectifiers and buck converters requires full-size converters but operates without energy curtailment.

References

[1] S. Lundberg, "Evaluation of wind farm layouts," *EPE J,* vol. 16, no. 1, pp. 14–21, Feb. 2006.

[2] P. Bresesti, W. L. Kling, R. L. Hendriks, and R. Vailati, "HVDC connection of offshore wind farms to the transmission system," *IEEE Trans. Energy Convers.*, vol. 22, no. 1, pp. 37–43, Mar. 2007.

[3] H. J. Bahirat, B. A. Mork, and H. K. Høidalen, "Comparison of wind farm topologies for offshore applications," in *Proc. IEEE Power Energy Soc. Gen. Meeting*, 2012, pp. 1–8.

[4] N. Holtsmark, H. J. Bahirat, M. Molinas, B. A. Mork, and H. K. Hoidalen, "An All-DC offshore wind farm with series-connected turbines: An alternative to the classical parallel AC model?," *IEEE Trans. Ind. Electron.*, vol. 60, no. 6, pp. 2420–2428, Jun. 2013.

[5] A. B. Mogstad, M. Molinas, P. K. Olsen, and R. Nilsen, "A power conversion system for offshore wind parks," in *Proc. 34th Annu. Conf. IEEE Ind. Electron.*, 2008, pp. 2106–2112.

[6] A. Garcés and M. Molinas, "A study of efficiency in a reduced matrix converter for offshore wind farms," *IEEE Trans. Ind. Electron.*, vol. 59, no. 1, pp. 184–193, Jan. 2012.

[7] S. Nishikata and F. Tatsuta, "A new interconnecting method for wind turbine/generators in a wind farm and basic performances of the integrated system," *IEEE Trans. Ind. Electron.*, vol. 57, no. 2, pp. 468–475, Feb. 2010.

[8] M. Popat, B. Wu, F. Liu, and N. Zargari, "Coordinated control of cascaded current-source converter based offshore wind farm," *IEEE Trans. Sustain. Energy*, vol. 3, no. 3, pp. 557–565, Jul. 2012.

[9] D. Jovcic, "Offshore wind farm with a series multiterminal CSI HVDC," *Electr. Power Syst. Res.*, vol. 78, no. 4, pp. 747–755, Apr. 2008.

[10] H. J. Lee and S. K. Sul, "Wind power collection and transmission with series connected current source converters," in *Proc. 14th Eur. Conf. Power Electron. Appl.*, 2011, pp. 1–10.

[11] M. H. Johnson and D. C. Aliprantis, "Analysis of series-DC offshore wind plants with aerodynamic wake effects," *IEEE Trans. Sustain. Energy*, vol. 8, no. 4, pp. 1706–1714, Oct. 2017.

[12] K. Musasa, M. N. Gitau, and R. C. Bansal, "Performance analysis of power converter based active rectifier for an offshore wind park," *Electr. Power Compon. Syst.*, vol. 43, no. 8/10, pp. 1089–1099, Jun. 2015.

[13] E. Veilleux and P. W. Lehn, "Interconnection of direct-drive wind turbines using a series-connected DC grid," *IEEE Trans. Sustain. Energy*, vol. 5, no. 1, pp. 139–147, Jan. 2014, doi: 10.1109/TSTE.2013.2276616.

[14] M. Pape and M. Kazerani, "An offshore wind farm with DC collection system featuring differential power processing," *IEEE Trans. Energy Convers.*, vol. 35, no. 1, pp. 222–236, Mar. 2020.

[15] M. S. U. Khan, A. I. Maswood, K. Satpathi, M. T. Iqbal, and A. Tripathi, "Analysis of brushless wound rotor synchronous generator with unity power factor rectifier for series offshore DC wind power collection," in *Proc. 44th Annu. Conf. IEEE Ind. Electron. Soc.*, 2018, pp. 1693–1698.

[16] K. Yamashita and S. Nishikata, "Steady-state characteristics of self-excited synchronous generators with damper windings for current-source type wind farm," in *Proc. 20th Int. Conf. Elect. Mach. Syst.*, 2017, pp. 1–6.

[17] N. Kawabata, N. Kimura, T. Morizane, and H. Omori, "New modulation control of converter system applied for offshore wind farms," in *Proc. Int. Power Electron. Conf.*, 2018, pp. 2887–2894.

[18] Q. Wei, B. Wu, D. Xu, and N. R. Zargari, "Medium frequency transformer based configuration for voltage source converter based offshore wind farm," in *Proc. IEEE 8th Int. Power Electron. Motion Control Conf.*, 2016, pp. 3521–3525.

[19] G. Guo *et al.*, "Series-connected-based offshore wind farms with full-bridge modular multilevel converter as grid- and generator-side converters," *IEEE Trans. Ind. Electron.*, vol. 67, no. 4, pp. 2798–2809, Apr. 2020.

[20] G. H. Kim, M. H. Kang, J. H. Ahn, E.-H. Kim, and S. H. Chae, "Operation of DC series connected offshore wind farm by using tap changing transformer with MMC-HVDC," in *Proc. 5th Int. Conf. Renewable Energy, Gener. Appl.*, 2018, pp. 291–295.

[21] F. Rong, G. Wu, X. Li, S. Huang, and B. Zhou, "ALL-DC offshore wind farm with series-connected wind turbines to overcome unequal wind speeds," *IEEE Trans. Power Electron.*, vol. 34, no. 2, pp. 1370–1381, Feb. 2019.

[22] M. H. Johnson, D. C. Aliprantis, and H. Chen, "Offshore wind farm with DC collection system," in *Proc. IEEE Power Energy Conf. Illinois*, Feb. 2013, pp. 53–59.

[23] S. Lundberg, *Wind Farm Configuration and Energy Efficiency Studies: Series DC Versus AC Layouts*. Gothenburg, Sweden: Chalmers Univ. Technol., 2006.

[24] K. J. P. Macken, J. L. J. Driesen, and R. J. M. Belmans, "A DC bus system for connecting offshore wind turbines with the utility system," in *Proc. Eur. Wind Energy Conf.*, 2001, pp. 1030–1035.

[25] K. Musasa and N. I. Nwulu, "A novel concept for offshore wind-power plant with DC collection system based on radial-connected converter topology," *IEEE Access*, vol. 6, pp. 67217–67222, 2018.

[26] C. Sun, G. Shi, J. Zhang, and X. Cai, "PWM plus phase-shift controlled DC-DC converter for use in series-connected DC wind farm," in *Proc. 12th IET Int. Conf. AC DC Power Transmiss.*, 2016, pp. 1–6.

[27] H. J. Bahirat and B. A. Mork, "Operation of DC series–parallel connected offshore wind farm," *IEEE Trans. Sustain. Energy*, vol. 10, no. 2, pp. 596–603, Apr. 2019.

[28] P. Lakshmanan, J. Liang, and N. Jenkins, "Assessment of collection systems for HVDC connected offshore wind farms," *Electr. Power Syst. Res.*, vol. 129, pp. 75–82, Dec. 2015.

[29] E. Veilleux, "Interconnection of direct-drive wind turbines using a series connected DC grid," Master Thesis, Dept. Elect. Comput. Eng., Univ. Toronto, Toronto, ON, Canada, 2009, Accessed on: Jun. 14, 2016. [Online]. Available: https://tspace.library.utoronto.ca/bitstream/1807/18950/6/Veilleux_Etienne_200911_MASc_thesis.pdf

[30] H. Zhang, D. Flórez, C. Saudemont, and F. Gruson, "Improved overvoltage limitation control approach of a DC series offshore wind farm based on MMC," in *Proc. 18th Mediterranean Electrotech. Conf.*, 2016, pp. 1–6.

[31] H. Zhang, D. Flórez, C. Saudemont, and F. Gruson, "Control strategies of a dc based offshore wind farm with series connected collection grid," in *Proc. IEEE Int. Energy Conf.*, 2016, pp. 1–6.

[32] J. Guo, X. Wang, Z. Zhang, H. Li, P. Lakshmanan, and J. Liang, "Energy curtailment analysis of offshore wind farms with DC series-parallel collection systems," in *Proc. 5th Int. Conf. Electr. Utility Deregulation Restruct. Power Technol.*, 2015, pp. 2014–2019.

[33] G. Shi, Z. Wang, M. Zhu, X. Cai, and L. Yao, "Variable speed control of series-connected DC wind turbines based on generalized dynamic model," in *Proc. 2nd IET Renewable Power Gener. Conf.*, 2013, pp. 1–6.
[34] P. Lakshmanan, J. Guo, and J. Liang, "Energy curtailment of DC series–parallel connected offshore wind farms," *IET Renew. Power Gener.*, vol. 12, no. 5, pp. 576–584, 2018.
[35] G. Shi, J. Zhang, X. Cai, and M. Zhu, "Decoupling control of series-connected DC wind turbines with energy storage system for offshore DC wind farm," in *Proc. IEEE 7th Int. Symp. Power Electron. Distrib. Gener. Syst.*, 2016, pp. 1–6.
[36] M. H. Rashid, *Power Electronics Handbook Devices, Circuits, and Applications*. Burlington, MA, USA: Butterworth-Heinemann, 2011. Accessed on: May 11, 2015. [Online]. Available: http://app.knovel.com/web/toc.v/cid:kpPEHDCAE1/viewerType:toc/root_slug:power-electronics-handbook
[37] M. Pape and M. Kazerani, "Turbine startup and shutdown in wind farms featuring partial power processing converters," *IEEE Open Access J. Power Energy*, vol. 7, pp. 254–264, Jul. 2020.
[38] G. Guo, K. Zha, J. Zhang, Z. Wang, F. Zhang, and J. Cao, "Grounding fault in series-connection-based offshore wind farms: Fault clearance," *IEEE Trans. Power Electron.*, vol. 35, no. 9, pp. 9357–9367, Sep. 2020.
[39] J. Jonkman, S. Butterfield, W. Musial, and G. Scott, "Definition of a 5-MW reference wind turbine for offshore system development," Tech. Rep. NREL/TP-500-38060, 947422, Feb. 2009.
[40] J. D. Grunnet, M. Soltani, T. Knudsen, M. Kragelund, and T. Bak, "Aeolus toolbox for dynamics wind farm model, simulation and control," in *Proc. Eur. Wind Energy Conf. Exhib. (EWEC)*, 2010.
[41] H. Li, Z. Chen, and H. Polinder, "Optimization of multibrid permanent-magnet wind generator systems," *IEEE Trans. Energy Convers.*, vol. 24, no. 1, pp. 82–92, Mar. 2009.
[42] A. K. Jain and R. Ayyanar, "Pwm control of dual active bridge: Comprehensive analysis and experimental verification," *IEEE Trans. Power Electron.*, vol. 26, no. 4, pp. 1215–1227, Apr. 2011.
[43] M. Pape and M. Kazerani, "On the efficiency of series-connected offshore DC wind farm configurations," in *Proc. IEEE Energy Convers. Congr. Expo.*, 2019, pp. 921–926.
[44] N. Mohan, T. M. Undeland, and W. P. Robbins, *Power Electronics - Converters, Applications, and Design*, 3rd ed., 2003.

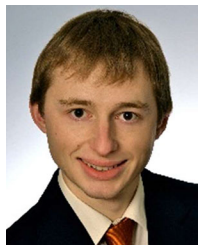

Marten Pape (Graduate Student Member, IEEE) received the B.Eng. degree in communications engineering and information technology from the Karlsruhe University of Applied Sciences, Karlsruhe, Germany, in 2012, and the M.A.Sc. degree in electrical and computer engineering in 2015 from the University of Waterloo, Waterloo, Canada, where he is currently working toward the Ph.D. degree with Power Electronics Research Group.

His research interests include the application of power electronic converters to renewable energy-driven power systems and distributed generation, design and control of power electronic converters, and microgrids.

Mehrdad Kazerani (Senior Member, IEEE) received the B.Sc. degree from Shiraz University, Shiraz, Iran, in 1980, the master's degree from Concordia University, Edmonton, AB, Canada, in 1990, and the Ph.D. degree from McGill University, Montreal, QC, Canada, in 1995, all in electrical engineering.

From 1982 to 1987, he was with the Energy Ministry of Iran. He is currently a Professor with the Department of Electrical and Computer Engineering, University of Waterloo, Waterloo, ON, Canada. He is a registered Professional Engineer with the province of Ontario. His research interests include current-sourced converter applications, matrix converters, distributed generation, energy storage, battery charging systems, electrified powertrains, and microgrids.